Analytic optimization of *Plasmodium falciparum* marker gene haplotype recovery from amplicon deep sequencing of complex mixtures

Authors

Zena Lapp, PhD[1]

Elizabeth Freedman[2]

Kathie Huang[2]

Christine F Markwalter, PhD[1]

Andrew A Obala, PhD[3]

Wendy Prudhomme-O'Meara, PhD[1,2]

Steve M Taylor, MD MPH[1,2]

[1]Duke Global Health Institute, Duke University, Durham, NC, USA

[2]Division of Infectious Diseases, School of Medicine, Duke University, Durham, NC, USA

[3]School of Medicine, College of Health Sciences, Moi University, Eldoret, Kenya

Short title: *P. falciparum* marker gene haplotype recovery from AmpSeq of complex mixtures

Abstract

Molecular epidemiologic studies of malaria parasites commonly employ amplicon deep sequencing (AmpSeq) of marker genes derived from dried blood spots (DBS) to answer public health questions related to topics such as transmission and drug resistance. As these methods are increasingly employed to inform direct public health action, it is important to rigorously evaluate the risk of false positive and false negative haplotypes derived from clinically-relevant sample types. We performed a control experiment evaluating haplotype recovery from AmpSeq of 5 marker genes (*ama1*, *csp*, *msp7*, *sera2*, and *trap*) from DBS containing mixtures of DNA from 1 to 10 known *P. falciparum* reference strains across 3 parasite densities in triplicate (n=270 samples). While false positive haplotypes were present across all parasite densities and mixtures, we optimized censoring criteria to remove 83% (148/179) of false positives while removing only 8% (67/859) of true positives. Post-censoring, the median pairwise Jaccard distance between replicates was 0.83. We failed to recover 35% (477/1365) of haplotypes expected to be present in the sample. Haplotypes were more likely to be missed in low-density samples with <1.5 genomes/μL (OR: 3.88, CI: 1.82-8.27, vs. high-density samples with ≥75 genomes/μL) and in samples with lower read depth (OR per 10,000 reads: 0.61, CI: 0.54-0.69). Furthermore, minority haplotypes within a sample were more likely to be missed than dominant haplotypes (OR per 0.01 increase in proportion: 0.96, CI: 0.96-0.97). Finally, in clinical samples the percent concordance across markers for multiplicity of infection ranged from 40%-80%. Taken together, our observations indicate that, with sufficient read depth, haplotypes can be successfully recovered from DBS while limiting the false positive rate.

Introduction

Malaria parasite surveillance and molecular epidemiologic studies increasingly employ as a genotyping approach amplicon deep sequencing (AmpSeq) of short polymorphic fragments of parasite DNA. Depending on which segments of the genome are sequenced, this approach returns haplotypes that can be used to estimate complexity of infection (1), investigate transmission between hosts (2,3), evaluate the prevalence and incidence of markers of drug resistance (4–6), and classify recurrent infections following drug treatment as reinfections or recrudescences (7,8). As a result of these diverse use cases of AmpSeq, there is a broad need for practical and empirically-derived approaches to maximize haplotype recovery and mitigate the risks of false genotypes.

Prior groups have evaluated the accuracy of haplotype recovery from mixtures containing DNA from known *P. falciparum* strains across a range of available tools and parameters, and reported that strains present in low proportions are likely to be missed (2,9) and that false positive haplotypes often have lower read depth (10,11). In a large analysis of complex mixtures of up to five reference strains, recovery of two markers was compared using four haplotype calling tools (11). They found that fewer haplotypes are recovered from samples with less *P. falciparum* DNA, that haplotypes with a lower read count were more frequently false positives, and that the four different haplotype calling tools performed similarly. What remains unexplored by these prior reports are investigations of haplotype recovery from samples with three key features of field studies: i) prepared and processed as dried blood spots (DBS), ii) present across a range of densities reflective of infections that are typically observed in field studies, and iii) harboring genomes from a large range of *P. falciparum* strains, which in natural infections can exceed 15 (2).

We evaluated the accuracy of the recovery of diverse *P. falciparum* haplotypes from DBS harboring simple and complex mixtures of parasite genomes. To do so, we prepared mixtures of up to 10 parasite strains at known proportions and across three parasite density categories, and amplified and sequenced each in triplicate with MiSeq across polymorphic segments of five distinct markers (*ama1*, *csp*, *msp7*, *sera2*, and *trap*). With these reads, we investigated the influence of parasite density, genomic complexity, and haplotype censoring criteria on the removal of false positive haplotypes, the sensitivity and precision of haplotype discovery, inter-replicate variability, and the ability to recover expected haplotypes at each locus.

Materials and Methods

Mock Infection design

We selected five targets of interest in the *P. falciparum* genome that have been used in prior AmpSeq studies (2,7,12): *ama1, csp, msp7, sera2,* and *trap*. We amplified by PCR using the reference primers for each (**Table 1**) from each of ten reference *P. falciparum* strain genomic DNAs (gDNAs): MRA-102G (3D7), MRA-150G (Dd2), MRA-152G (7g8), MRA-155G (HB3), MRA-159G (K1), MRA-176G (V1/S), MRA-1169G (Tanzania), MRA-915G (FUP UGANDA-Palo Alto), MRA-309G (FCB), and MRA-731G (FCR3/Gambia). The products of each were Sanger sequenced to determine the reference sequence for each strain.

Table 1: Marker-specific reference primers

Marker	Forward primer	Reverse primer
ama1	TCAGGGAAATGTCCAGTATTTG	GGACCATTATTTTCTTGAGCTG
csp	TTAAGGAACAAGAAGGATAATACCA	AAATGACCCAAACCGAAATG
msp7	ATGAACAAGAGATATCAACACA	TTAAATTGTTCATGGTATTCCTTA
sera2	TACTTTCCCTTGCCCTTGTG	CACTACAGATGAATCTGCTACAGGA
trap	TCCAGCACATGCGAGTAAAG	AAACCCGAAAATAAGCACGA

For each reference strain and marker, Unipro UGENE v42 (13) was used to map forward and reverse reads from Sanger sequencing to the respective marker gene. The trimming quality threshold and mapping minimum similarity were set to zero. The sequences were manually trimmed and, where discrepancies in base calls were observed between forward and reverse reads, bases were called manually.

Five mock polygenomic infections and a 3D7-only mock infection were created by making control mixtures that combined 1 ng/µl gDNA stocks of the distinct parasite reference strains in known percentages ranging from 1% to 100% (**Figure 1A**). Each control mixture was serially diluted in uninfected whole blood, and dried blood spots (DBSs) were made for each of the 11 dilutions per mixture. DBS were singly punched into individual wells of a deep 96-well plate, and a modified Chelex-100 protocol (3) was used to make gDNA extracts. These were then tested in duplicate with a duplex pfr364/human β-tubulin quantitative PCR (qPCR) assay that estimated parasite densities using a standard curve generated with extracts from control DBS at dilutions of *P. falciparum* 3D7 ranging from 0.1 to 2000 parasites/µL of whole blood (14). Control mixture extracts were assigned to one of three parasite density ranges (low, <1.5 genomes/µl; medium, 1.5-75 genomes/µl; and high, ≥75 genomes/µl) and pooled by mixture at each density range for a total 18 pools (6 mixtures x 3 densities) to be used as templates for subsequent PCR amplification.

Library preparation and sequencing

Each mixture template was prepared for sequencing according to qPCR Ct-value as described in (3). Then, from each mixture template, we amplified at the target segments of *ama1, csp, msp7, sera2*, and *trap* in individual reactions in triplicate using a nested PCR strategy. Library preparation for sequencing followed described methods (15) with the following exceptions: PCR1 reactions included 300nM of each primer and 7 µl of template gDNA when extract Ct was < 28 (high density), 18 µl when 28 ≤ Ct < 34 (medium density), and 15 µl concentrated extract when Ct ≥ 34 (low density). PCR 1 cycling conditions were 95C x 3′ → (98C × 20s → 62C × 15s → 72C × 20s) × 8 → (98C × 20s →70C × 15s → 72C × 20s) x 27 → 72C × 1′. PCR 2 reactions included 2 µl of template when gDNA pool extract Ct was < 28, and 8 µl of template when Ct was ≥ 28. The resulting dual-indexed libraries were then pooled and purified as

previously described (15) before sequencing on an Illumina MiSeq (v3 300PE) platform. Raw sequences have been deposited under BioProject PRJNAXXX.

Haplotype recovery

We used Snakemake v 7.20.0 (16) to build an integrated pipeline for haplotype recovery, BRAVA (Basic and Rigorous Amplicon Variant Analyzer; https://github.com/duke-malaria-collaboratory/BRAVA) in order to trim, filter, and map reads, and thence call haplotypes. Primers and adapters of amplicon deep sequencing reads for each marker were removed using Cutadapt v4.1 (17). These reads were trimmed using Trimmomatic v0.38 (18); this removed the leading and trailing bases below a Phred quality score of 10, removed all nucleotides from the 3' end after the quality of the read falls below an average Phred quality score of 15 over a sliding window of 4 nucleotides, and dropped reads with fewer than 80 nucleotides. Remaining reads were mapped to the 3D7 reference genome using BBmap v39.01 (19). Reads were then further filtered and trimmed using the R package DADA2 v1.20.0 (20) function filterAndTrim with a maximum number of expected errors (maxEE) equal to 1. Values ranging from 2 to 10 were tested for the truncQ parameter in filterAndTrim, which truncates reads at the first instance of a quality score ≤truncQ. The optimal value was determined to be the value that maximized the number of reads used for haplotype calling (10); the haplotypes that were output when using this value of truncQ were used for all subsequent analyses. Next, the learnErrors function was used to learn error rates, the dada function was used to remove sequencing errors and identify haplotypes, and the removeBimeraDenovo function was used to remove chimeras. All haplotypes returned by DADA2 were included for analysis.

Categorization of haplotypes

For each locus in each sample, we categorized each haplotype returned by DADA2 into one of three groups:

1. Expected haplotype: A haplotype with an identical sequence to that of a template sequence expected to be observed in the sequenced library. These were considered *true positive haplotypes.*
2. Haplotype arising from systematic error: A haplotype with a sequence or read depth that we did not expect to observe in the sequenced library, but which was observed across all three replicates for at least one density bin. These were suspected to be truly present owing to either inadvertent introduction to mixtures during gDNA preparation or the presence of multiple haplotypes in the original source gDNA. Haplotypes arising from systematic error were removed from the analysis prior to screening for optimal thresholds for haplotype censoring, as we suspected that these template strains were truly present in the library that was sequenced and therefore shouldn't be expected to be corrected by applying filtering criteria.
3. Haplotype arising from random error: A haplotype that we did not expect to observe in the sequenced library, and that was not consistently present across replicates for any mixture-density combination. These were considered *false positive haplotypes*.

Identification of optimal thresholds for haplotype censoring

We evaluated the efficacy of four common metrics used to censor haplotypes: i) the depth of reads within a sample supporting a haplotype (read depth), ii) the proportion of reads within a sample supporting a haplotype (read proportion), iii) the ratio of abundances of pairs of haplotypes within a sample with a Hamming distance of one (read ratio), and iv) the length difference of the returned haplotype relative to that of the expected reference strain (length difference). As mentioned above, haplotypes arising from systematic error were removed prior to evaluating these criteria. All reference strain haplotypes for all loci were identical in length to the 3D7 haplotype, except one *msp7* haplotype that was 3 base pairs shorter. Thus, we defined this censoring criterion as follows: the difference in length between the observed haplotype and

the 3D7 reference haplotype must be equal to 0, -3, or 3 (i.e. one codon may be inserted or deleted). For the other 3 censoring criteria, we used Youden's J statistic to identify optimal thresholds across all possible thresholds of the criterion and corresponding confidence intervals with the coords and ci.coords functions from the R package pROC v1.18.0 (21). Because the importance of retaining true positive haplotypes vs. removing false positive haplotypes varies depending on the use case, this statistic was computed using three different ways to weight false negative vs. false positive classifications: equal weight to false negatives and false positives, 2x the weight to false negatives, and 2x the weight to false positives. To evaluate censoring criteria, we used the optimal criteria based on false negatives having 2x the cost of false positives.

Risk factor analysis for missing haplotypes

We performed a bivariate and multivariate logistic regression to investigate risk factors for haplotype missingness in R using the glmer function in lme4 v1.1.32 (22). Missing haplotypes were defined as those that were not observed in the sample prior to the application of any haplotype censoring criteria. The outcome was the presence or absence of the haplotype in the un-censored haplotypes, and covariates were target, starting proportion of the reference template strain, read depth (per 10,000 reads), parasite density, and expected number of distinct haplotypes present in the sample. A random intercept was included for each mixture-density combination. Low-density mix C samples were excluded from this analysis as they exhibited signatures of contamination from a high-density sample.

Clinical sample analysis

Ten *P. falciparum*-positive DBS collected in a field study in Webuye, Kenya that were previously sequenced at the *ama1* and *csp* loci (2) were sequenced at the *msp7*, *sera2*, and *trap* loci. These samples were selected from those that were high-density and had MOIs >1 at both *ama1*

and *csp* loci (using previously defined haplotype calls and censoring criteria (2)). Haplotypes for newly sequenced loci were called with the pipeline described above, using the same method as for *ama1* and *csp*. All haplotypes were censored using the identified optimal censoring criteria.

Ethical statement

The field study in which the clinical samples were collected was approved by institutional review boards of Moi University (2017/36) and Duke University (Pro00082000). All participants or guardians provided written informed consent, and those over age 8 years provided additional assent.

Data analysis and visualization

All data were analyzed and visualized using R v4.2.1 (23) in RStudio v2022.12.0+353 (24) with the following packages: msa v1.28.0 (25), tidyverse v2.0.0 (26), readxl v1.4.2 (27), ape v5.7.1 (28), regentrans v1.0.0 (29), reshape2 v1.4.4 (30), scales v1.2.1 (31), cowplot v1.1.1 (32), ggupset v0.3.0 (33), broom.mixed v0.2.9.4 (34), ggpmisc v0.5.2 (35), ggpubr v0.6.0 (36), and ggtext v0.1.2 (37). Variant positions in the amplified portion of each marker gene were extracted from Pf6k (38) VCF files and tallied. We compared read depths of true and false positive haplotypes, and median multiplicities of infection, using a Wilcoxon test, and number of haplotypes censored by density using a Fisher's exact test. Code and data for this manuscript can be found at https://github.com/duke-malaria-collaboratory/brava_validation.

Results

Mixtures, reference strains, deep sequencing, and haplotype calling

We sequenced five previously-developed AmpSeq marker genes: *ama1*, *csp*, *msp7*, *sera2*, and *trap* (**Table 2**), and generated for sequencing 6 mock infections harboring mixtures of gDNA from between 1 and 10 distinct parasite reference strains (**Figure 1A**) to approximate the polygenomic nature of many infections in high-transmission areas. Not all marker genes were unique to a strain; a total of 37 distinct haplotypes were present across the 10 strains and 5 markers. Pairwise single nucleotide variant (SNV) distance varied between strains and markers (median: 4, range: 0-15; **Figure 1B**).

For each marker gene, each of the 6 mixtures was sequenced from dilution pools corresponding to low (<1.5 genomes/μL), medium (1.5-75 genomes/μL) and high (≥75 genomes/μL) parasite density bins in triplicate, tallying to 1365 expected haplotype occurrences across 270 sequenced samples. We obtained analyzable reads for 257/270 samples, with differences in the absolute yield of read counts between low (4.3 million), medium (8.0 million), and high (10.2 million) density samples. This general observation held for each individual marker, save for *trap* and *msp7* which returned moderate read amounts irrespective of parasite density bin (**Figure 1C**). Overall, we observed across the five loci and 257 samples 1292 haplotype occurrences (**Figure 1D**), for which the median read depth was 1542.

Table 2: Marker gene characteristics

Target	Stage expressed	3D7 gene ID	Chromosome	3D7 coordinates amplified	Sequence length	3D7 GC content	Number of Pf6k variant positions
ama1	Blood	PF3D7_1133400	11	1294312-1294613	300	27%	49 (16%)

csp	Liver	PF3D7_0304600	03	221351-221640	288	29%	53 (18%)
msp7	Blood	PF3D7_1335100	13	1419236-1419567	330	25%	53 (16%)
sera2	Blood	PF3D7_0207900	02	320762-321022	259	41%	62 (24%)
trap	Liver	PF3D7_1335900	13	1465058-1465379	320	31%	46 (14%)

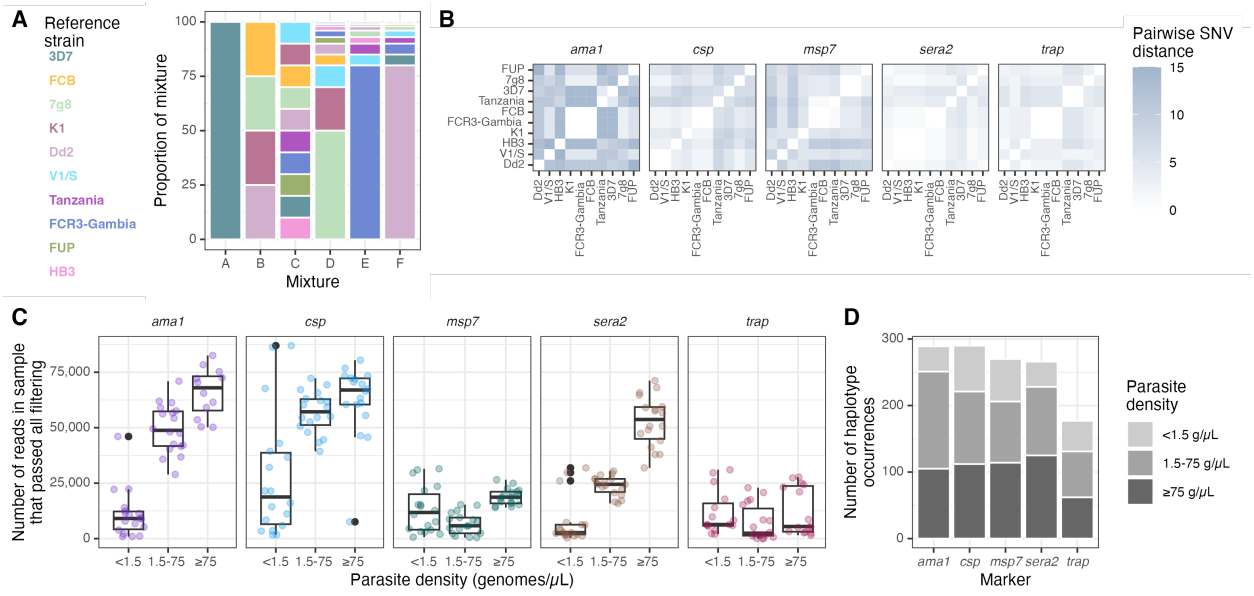

Figure 1: Overview of mixtures, reference strains, and sequence yield. (A) Overview of mixtures A through F, each composed of various proportions of gDNA from the listed *P. falciparum* reference strains (colors). **(B)** Pairwise single nucleotide variant (SNV) distances between reference haplotypes of each of the marker genes obtained by Sanger sequencing. **(C)** Number of reads in each sample by parasite density bin, faceted by marker gene. **(D)** Total number of pre-censored haplotype occurrences for each marker across all mixtures and replicates, colored by parasite density bin. Note that *ama1* was sequenced separately from the

244 other markers so read depth cannot be directly compared between *ama1* and other markers.
245 g/μL = genomes/µL.
246
247 **False positive haplotypes**
248 We first investigated false positive haplotype occurrences across samples. Within each sample,
249 we categorized each observed haplotype as expected to be present in the sample (true positive,
250 n=859/1292, 66%), likely cryptically present in the original mixture (systematic error;
251 n=254/1292, 20%), or likely arising from random error (false positive, n=179/1292, 14%) (**Figure**
252 **2A**). Only 1% of reads that passed filtering supported haplotypes that were categorized as false
253 positives. We observed this trend of proportionately few reads supporting proportionately more
254 false positive haplotypes across both markers and parasite density bins (**Figure 2B**).
255 Furthermore, the percentage of false positive haplotypes was relatively similar across parasite
256 density bin (12-16%), although for *ama1* and *sera2*, there were fewer false positive haplotypes
257 for low-density templates (**Figure 2C**). False positive haplotypes were often not the correct
258 sequence length, were often only one nucleotide different from a reference sequence in the
259 sample (**Figure 2C**), and had lower read depths than haplotypes we expected to observe
260 (median=104 vs. 2393, Wilcox $p < 0.001$; **Figure 2D**).

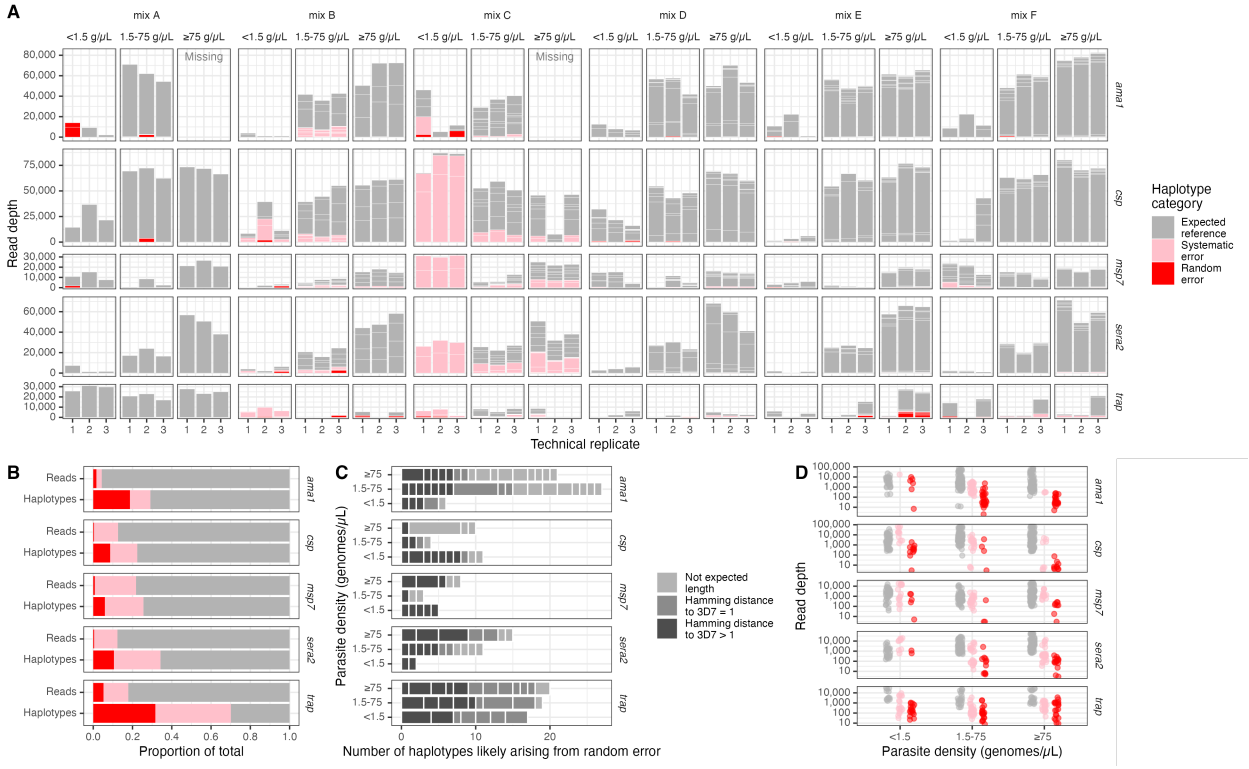

Figure 2: Overview of false positive haplotypes. (A) Sample-level haplotype overview. Stacked boxes in each column represent observed haplotypes from reads that passed filtering, categorized as those expected in the reference (gray), arising from systematic error (pink), or from random error (red). Box heights indicate the number of reads supporting the haplotype. **(B)** Proportion of reads and of haplotypes by marker categorized as expected reference, systematic error, and random error. **(C)** False positive haplotypes by marker categorized by unexpected length and by SNV distance to the 3D7 reference sequence. Hamming distances were only computed for haplotypes identical in length to the 3D7 reference sequence. **(D)** Read depth for expected (gray), systematic error (pink) and random error (red) haplotypes by parasite density bin and by marker. g/µL = genomes/µL.

Evaluating haplotype censoring criteria

We next evaluated, in our dataset, the effectiveness of four important threshold criteria typically applied to remove false positives from AmpSeq data: read depth, read proportion, read ratio of

similar haplotypes, and haplotype length. The optimal thresholds had large confidence intervals and varied depending on how much weight was given to false positive vs. false negative haplotypes (**Figure 3A-C**). Prioritizing the inclusion of true positive haplotypes over the removal of false positive haplotypes, optimal thresholds were 275 for read depth (95% CI: [204-420]; sensitivity = 0.95 [0.90-0.99]; specificity = 0.52 [0.46-0.68]), 0.007 for read proportion (95% CI: [0.005-0.014]; sensitivity = 0.97 [0.91-0.99]; specificity = 0.54 [0.47-0.69]), and 0.21 for read ratio (95% CI: [0.09-0.36]; sensitivity = 0.82 [0.72-0.93]; specificity = 0.67 [0.44-0.67]). Using these criteria, across all targets 975/1292 (75%) haplotype occurrences remained corresponding to 59/124 (48%) distinct haplotypes, yielding at least one uncensored haplotype in 254/257 (99%) samples. Specifically, these thresholds censored 148/179 (83%) random error haplotypes, 102/254 (40%) systematic error haplotypes, and 67/859 (8%) expected reference haplotypes (**Figure 3D-E**). Of the 179 random error haplotypes, 75% fell under the read threshold, 54% fell under the proportion threshold, 30% fell under the within-sample ratio threshold, and 28% had a length different than the reference strains. Furthermore, for all markers but *trap*, fewer false positive haplotypes were successfully censored in lower parasite density bins (Fisher's exact $p < 0.01$, **Figure 3F**), yielding more false positives post-censoring in low- (11) compared to medium- (6) and high-density (0) parasite bins. Of the censored true positive haplotypes, over half (39/67; 58%) were from high-density templates, and only 5/67 (7%) made up ≥10% of the original mixture (**Figure 3G**).

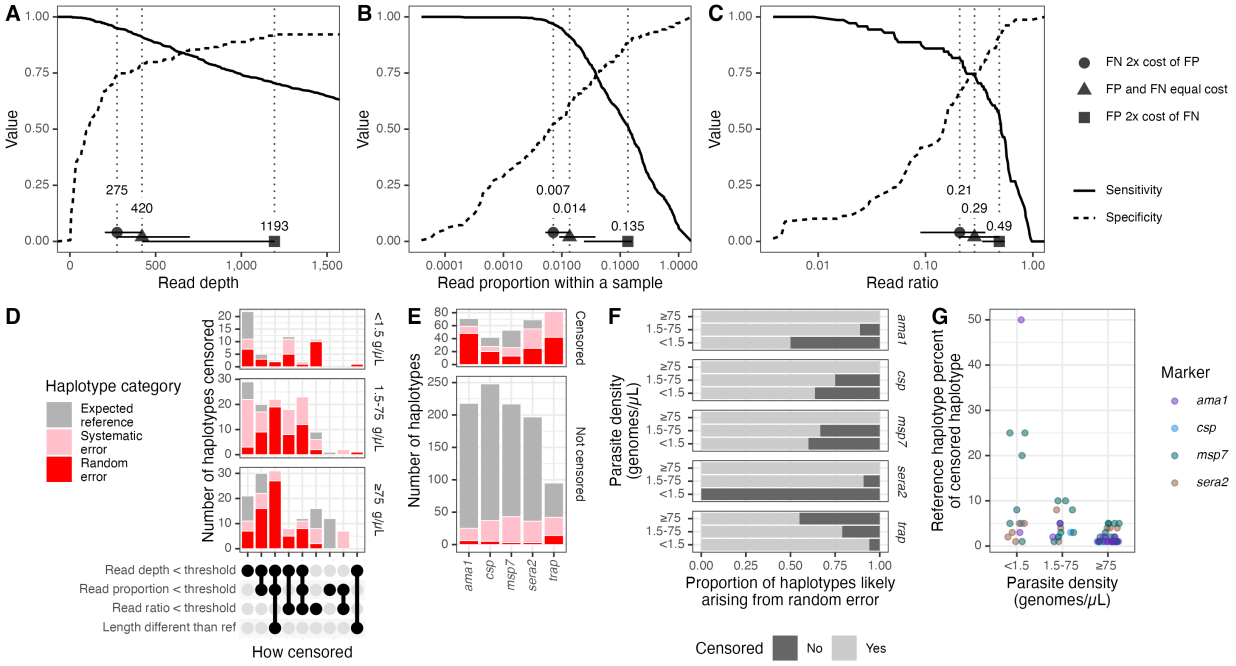

Figure 3: Optimization and application of censoring criteria. (A-C) Sensitivity and specificity across ranges of tested thresholds for haplotype **(A)** read depth, **(B)** read proportion, and **(C)** ratio within a sample between haplotypes with a Hamming distance of 1. **(D)** Count of censored haplotypes by the criterion by which they were censored and by density of parasites in DBS sample. The majority of censored haplotypes were non-reference haplotypes and fell under the identified read depth threshold. **(E)** Numbers of censored and uncensored haplotypes by haplotype category and by marker. **(F)** Proportion of uncensored (light grey) and censored (dark grey) haplotypes likely arising from random error, by parasite density bin and marker. **(G)** Reference haplotype percent of censored haplotypes. No reference haplotypes were censored out for *trap*. g/µL = genomes/µL. FN = false negative; FP = false positive. g/µL = genomes/µL.

Inter-replicate variability

To evaluate the consistency with which haplotypes were returned, we measured inter-replicate variability post-censoring. Overall, 58% of haplotypes were observed in all 3 replicates, 18% in 2 replicates, and 24% in 1 replicate. Haplotypes were more consistently returned in all three

311 replicates for high-density samples (76% of the time) compared to medium- (61% of the time)
312 and low-density samples (30% of the time) (**Figure 4A**). Consistent with this, in high-density
313 samples Jaccard distances between replicates were higher (median = 1, IQR = 0.2) compared
314 to medium- (median = 0.83, IQR = 0.5) and low-density samples (median = 0.5, IQR = 0.75)
315 (**Figure 4B**).
316

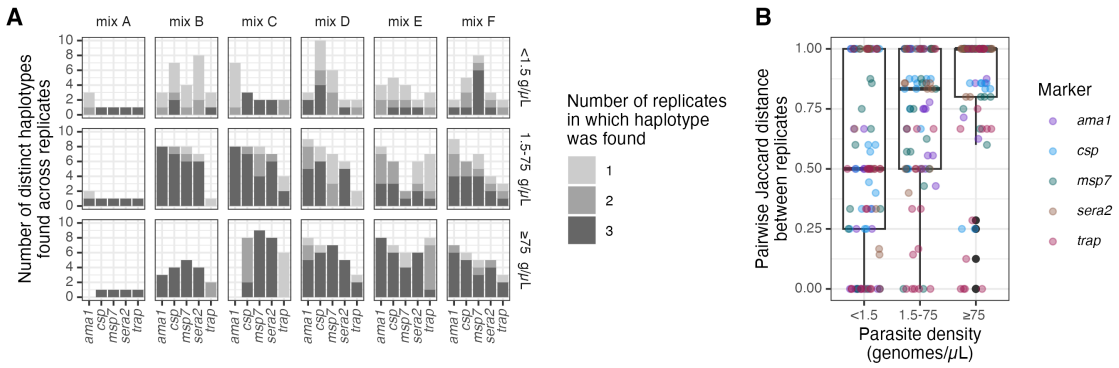

317

318 **Figure 4: Inter-replicate variability. (A)** Number of replicates in which each haplotype was
319 found (color) by mix, parasite density bin, and target. **(B)** Pairwise Jaccard distance between
320 replicates by parasite density bin, colored by marker. g/µL = genomes/µL.
321

322 **Missing haplotypes**

323 Of the 1365 haplotype occurrences expected to be present across all samples, we did not
324 recover 477 (35%). Thus, we next investigated factors associated with missing haplotypes. As
325 expected, haplotype proportion within a sample was inversely associated with missingness, with
326 each increase of 0.01 in proportion associated with a 4% reduction in the likelihood of being
327 missed (OR: 0.96, 95% CI: 0.96-0.97), even when controlling for marker, density bin, number of
328 reads in the sample, and expected number of haplotypes (**Figure 5A**; **Table 3**). Additionally, for
329 all markers except *trap*, <15% of haplotypes were missed from high-density samples, while
330 >45% were missed from low-density samples (**Fig 5A**). Overall read depth for a sample was
331 negatively correlated with the proportion of haplotypes that were missing from the sample

(Spearman's rho = -0.62; **Figure 5B**). Furthermore, within a sample, observed and expected read proportions were correlated, although there was high stochasticity, particularly for the low-density samples (**Figure 5C**). Finally, in high-density samples only 30/166 (18%) haplotypes were not recovered in any replicates, while in low-density samples 78/158 (49%) were not recovered in any replicates (**Figure 5D**).

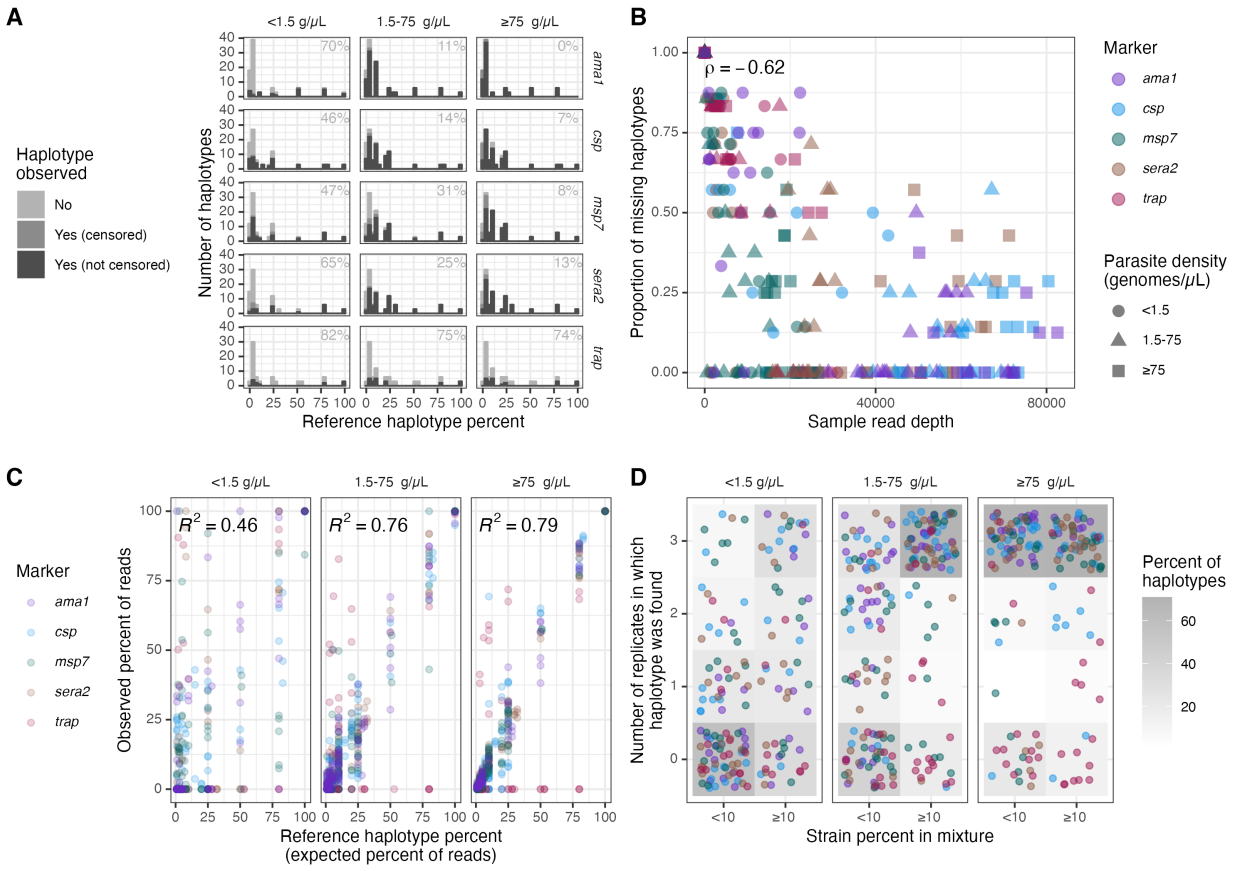

Figure 5: Summary of missing haplotypes. (A) Numbers of missing haplotypes (light grey), observed but censored haplotypes (medium grey), and observed haplotypes (dark grey) in individual samples by marker and parasite density bin. The number in each facet indicates the percentage of missing haplotypes. All subsequent panels in this figure consider observed but censored haplotypes as missing. **(B)** Correlation between the overall read depth of a sample and proportion of all expected haplotypes within a mixture that were not successfully recovered.

Color indicates marker, and shape indicates parasite density. Spearman's rho = -0.62. **(C)** Correlation between proportions of expected and observed haplotypes within individual samples by parasite density bin, colored by marker**. (D)** Number of replicates in which the haplotype was found by binned strain percent in the original mixture (present at <10% or ≥10%). Each point is a haplotype colored by marker. The grey color beneath the points indicates the percent of haplotypes across all targets and mixtures in a given strain percent bin that were observed in the corresponding number of replicates. Low-density mix C samples were excluded from this figure as they exhibited signatures of contamination from a high-density sample. g/µL = genomes/µL.

Table 3: Risk factors for haplotype missingness

Feature	Term	Bivariate Odds Ratio (95% CI)	Multivariate Odds Ratio (95% CI)*
Haplotype proportion (per 0.01 increase)		0.98 (0.97-0.98); p=4.3e-11	0.96 (0.96-0.97); p=6e-17
Target	*ama1*	REF	REF
	csp	0.76 (0.49-1.18); p=0.23	0.90 (0.54-1.51); p=0.7
	msp7	1.24 (0.81-1.89); p=0.32	0.40 (0.23-0.68); p=8e-04
	sera2	1.68 (1.1-2.57); p=0.016	1.05 (0.63-1.77); p=0.8
	trap	21.37 (13.02-35.08); p=1e-33	6.13 (3.13-12.03); p=1e-07
Density, genomes/µL	≥75	REF	REF
	1.5-75	1.62 (0.76-3.45); p=0.21	1.47 (0.75-2.88); p=0.3
	<1.5	6.27 (2.87-13.69); p=3.9e-06	3.88 (1.82-8.27); p=5e-04
Read depth (per 10,000 reads)		0.57 (0.53-0.62); p=5.7e-40	0.61 (0.54-0.69); p=3e-15

Feature	Term	Bivariate Odds Ratio (95% CI)	Multivariate Odds Ratio (95% CI)*
Expected number of haplotypes		0.32 (0.24-0.44); p=1.2e-12	1.08 (0.91-1.27); p=0.4

* Covariates included were haplotype proportion, target, parasite density, read depth, and expected number of haplotypes

Estimating multiplicity of infection based on marker haplotype diversity

We next compared the expected multiplicity of infection (MOI) to the observed MOI after censoring, with MOI expressed as the number of haplotypes observed at each individual marker. Relative to the expected MOIs, the observed MOIs were equal 29% (74/254) of the time, lower 61% (154/254) of the time, and higher only 10% (26/254) of the time. MOIs were more likely to be underestimated in low-density samples (median observed-expected MOI = -4 for low-density samples vs. -1 for medium- and high- samples, Wilcox $p < 0.001$; **Figure 6A**). We performed a similar comparison using 10 high-density *P. falciparum* infections collected as DBS through a recent field study in Western Kenya, in order to capture a broader naturally-occurring diversity of marker haplotypes (2). Using the optimal censoring criteria defined above, we observed 142 haplotypes across all samples and markers, of which 36 (25%) were censored. The range of MOIs was 1-5 for each marker. No marker consistently estimated the highest or lowest MOI, and the percent concordance ranged from 40% to 80% (**Figure 6B**).

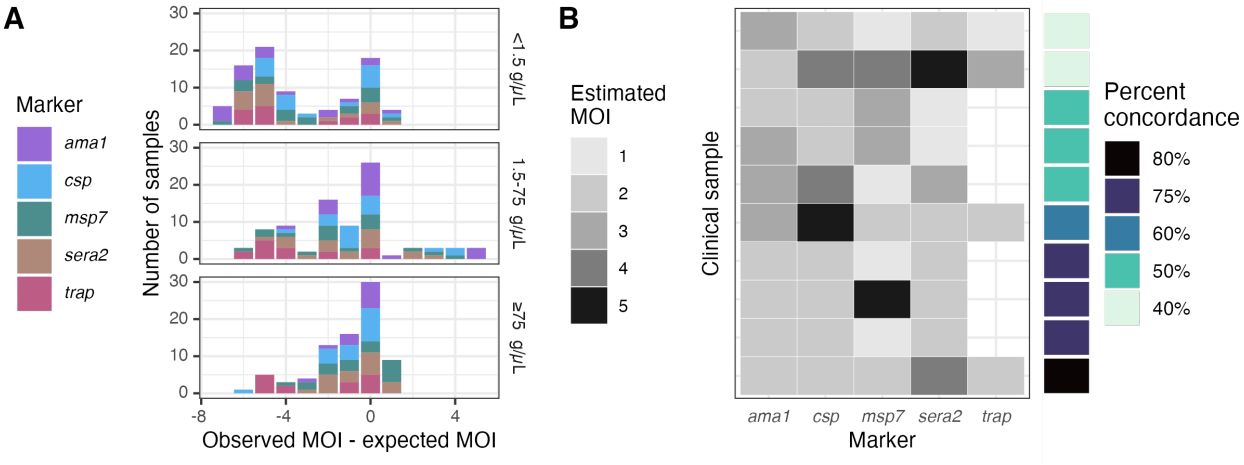

Figure 6: Estimated multiplicities of infection (MOIs) based on each marker haplotype. (A) Observed minus expected MOIs for mixtures post-censoring. **(B)** Estimated MOIs in clinical samples. Haplotypes were censored according to the optimal criteria identified above, giving false negatives 2x the cost of false positives. Not all *trap* clinical samples returned sequences. Percent concordance was computed for each sample as the percentage of markers for which the estimated MOI was equal to the mode MOI.

Discussion

AmpSeq is an increasingly popular tool for molecular epidemiologic studies of *P. falciparum* collected on DBS, which necessitates rigorous haplotype recovery from field samples. We prepared DBS containing mixtures of gDNA from reference *P. falciparum* strains, amplified and sequenced polymorphic segments of 5 common marker genes in triplicate, and quantified the performance of haplotype recovery using a range of metrics. We observed that high sample read depth was associated with enhanced recovery of most haplotypes present in the original sample, and that censoring criteria based on read depth, read proportion, read ratio, and haplotype length can effectively remove most false positive haplotypes while retaining most true positive haplotypes. Thus, for use-cases which involve high-density samples or samples sequenced at high read depth, rigorous recovery can be achieved for multiple markers.

Consistent with prior studies (2,9,11), we observed that the likelihood of haplotype recovery is enhanced by higher parasite density and by a larger proportion of an individual haplotype within a mixture. In particular, the consistency with which we observed haplotypes across replicates was higher in high-density samples compared to low-density samples. However, we further observed that, independent of parasite density and reference haplotype proportion, successful haplotype recovery was further associated with a higher overall sample read depth. The ability to recover haplotypes constituting a minority population within a parasitemia with an overall low density is an important goal for many use cases of AmpSeq. Namely, therapeutic efficacy studies of antimalarials use active case detection to screen for recurrence of parasites, and frequently capture low-density infections with multiple strains which must then be compared to those in the initial infection in order to distinguish reinfection from recrudescent infection (7). Additionally, studies of transmission networks in highly endemic settings in which low-density, asymptomatic infections predominate also benefit from comprehensive profiling of strains within mixtures in order to ascertain parasite relatedness between hosts (2). In these and similar use

cases, the likelihood of detecting minority haplotypes can be improved by maximizing per-sample read depth, such as by limiting multiplexing and selecting maximal sequencing platform output.

We observed very different optimal censoring thresholds depending on how we weighted the relative importance of false positive and false negative haplotypes, which highlights the need to select censoring criteria suitable for the primary study objective. Penalizing false negative haplotypes more than false positive haplotypes yielded haplotype censoring criteria that still managed to remove most false positive haplotypes while retaining high sensitivity. Furthermore, these criteria were consistent with thresholds that others have used and reported in the literature (read depth: 204-420, read proportion: 0.005-0.014, read ratio: 0.09-0.36) (2,11).

We observed inconsistency in performance between markers with respect to false positives, censoring, missingness, and MOI. Pre-censoring, false-positive haplotypes were rarely recovered for *msp7* but common for *ama1* and *trap*. However, post-censoring the number of false positives was relatively low for all markers but *trap*. Fewer haplotypes were recovered for *sera2* and *trap* overall. Furthermore, there was no consistent trend across a limited set of clinical samples of marker-specific MOI, suggesting that MOI estimates based upon a single marker may frequently underestimate the true MOI of a sample, as previously described (11). Since most markers returned largely correct haplotype calls across a range of mixtures and parasite density bins, choice of marker may depend not only on marker performance but also other factors such as the biological question of interest (e.g. transmission, vaccine development, etc.).

Despite controlled laboratory conditions, we observed signatures of both systematic and random error. Systematic error may have resulted from two different sources. First, it is possible

that multiple haplotypes were present in the original template strains and were missed during Sanger sequencing. Second, systematic error could arise from contamination during gDNA extraction. Owing to the high-throughput manner of DBS processing, using 96-well plates, it is unfortunate but expected that we observe contamination in a small minority of samples included in a sequencing run. This highlights the importance of meticulous laboratory work and thoughtful controls, particularly because these haplotypes are less likely to be removed by censoring criteria owing to their presence in the original template. In contrast, random error may arise due to PCR stochasticity and polymerase error in low-input next-generation sequencing libraries (39). This is also inevitable, and the censoring criteria described here successfully removed many haplotypes arising from these technical errors.

Our study had several limitations. First, we created the mixtures from gDNA rather than from intracellular DNA; therefore, the composition of the solution from which DNA was amplified was slightly less complex than that from clinical samples. However, as we extracted DNA from DBS, our results provide a closer approximation to clinical samples than previous studies. Second, we did not attempt to censor haplotypes arising from systematic error because the commonly used censoring criteria assessed here assume that false positive haplotypes arise from random rather than systematic error. Third, this study focused on in silico recovery of haplotypes, and replicates were drawn from the same gDNA extract pools. Thus, variability occurring due to extraction is not accounted for in these data. However, our results provide useful insight into variation and random errors occurring at the amplification and sequencing steps.

Conclusions

We observed that *P. falciparum* haplotypes from multiple different targets can be successfully recovered from DBS, that in the majority of cases these haplotypes are recovered across

458 replicates, and that censoring criteria already used by the community remove most false

459 positive haplotypes while retaining high sensitivity.

Funding

This work was supported by the National Institute of Allergy and Infectious Diseases (R01AI146849 to W.P-O. and S.M.T. and K01AI175527 to C.F.M.)

Acknowledgements

We thank Jenna DeCurzio for helping with the preparation of samples for sequencing, as well as Laura-Leigh Rowlette and Fangfei Ye at the Duke University Sequencing & Genomic Technologies Shared Resource for performing sequencing and preliminary processing of sequenced reads. *P. falciparum* strains 3D7 (MRA-102, contributed by Daniel J. Carucci), FUP UGANDA-PALO ALTO (MRA-915, contributed by T. Sam-Yellowe), Dd2 (MRA-150G, contributed by David Walliker), 7G8 (MRA-152G, contributed by David Walliker), HB3 (MRA-155G, contributed by Tom Wellems), K1 (MRA-159G, contributed by Dennis Kyle), V1/S (MRA-176G, contributed by Dennis Kyle), Tanzania (MRA-1169G, contributed by Michal Fried), FCB (MRA-309G, contributed by Tom Wellems), and FCR3/Gambia (MRA-731G, contributed by William Trager) were obtained from BEI Resources, NIAID, NIH.

Author contributions

ZL, EF, CFM, WPO, and SMT conceptualized the project. ZL, EF, and CFM developed methodology. EF performed the investigation. ZL and KH developed software. ZL performed data curation, formal analysis, and visualization. AAO, WPO, and SMT provided resources, supervision, project administration, and funding acquisition. ZL, EF, and SMT wrote the original draft. All authors reviewed and edited the manuscript.

References

1. Miller RH, Hathaway NJ, Kharabora O, Mwandagalirwa K, Tshefu A, Meshnick SR, et al. A deep sequencing approach to estimate Plasmodium falciparum complexity of infection (COI) and explore apical membrane antigen 1 diversity. Malaria Journal. 2017 Dec 16;16(1):490.

2. Sumner KM, Freedman E, Abel L, Obala A, Pence BW, Wesolowski A, et al. Genotyping cognate Plasmodium falciparum in humans and mosquitoes to estimate onward transmission of asymptomatic infections. Nat Commun. 2021 Feb 10;12(1):909.

3. Markwalter CF, Menya D, Wesolowski A, Esimit D, Lokoel G, Kipkoech J, et al. Plasmodium falciparum importation does not sustain malaria transmission in a semi-arid region of Kenya. PLOS Global Public Health. 2022 Aug 10;2(8):e0000807.

4. Niba PTN, Nji AM, Chedjou JPK, Hansson H, Hocke EF, Ali IM, et al. Evolution of Plasmodium falciparum antimalarial drug resistance markers post-adoption of artemisinin-based combination therapies in Yaounde, Cameroon. International Journal of Infectious Diseases. 2023 Jul 1;132:108–17.

5. Osoti V, Akinyi M, Wamae K, Kimenyi KM, de Laurent Z, Ndwiga L, et al. Targeted Amplicon Deep Sequencing for Monitoring Antimalarial Resistance Markers in Western Kenya. Antimicrobial Agents and Chemotherapy. 2022 Mar 10;66(4):e01945-21.

6. Olukosi AY, Ajibaye O, Omoniwa O, Oresanya O, Oluwagbemiga AO, Ujuju C, et al. Baseline prevalence of molecular marker of sulfadoxine/pyrimethamine resistance in Ebonyi and Osun states, Nigeria: amplicon deep sequencing of dhps-540. Journal of Antimicrobial Chemotherapy. 2023 Mar 2;78(3):788–91.

7. Gruenberg M, Lerch A, Beck HP, Felger I. Amplicon deep sequencing improves Plasmodium falciparum genotyping in clinical trials of antimalarial drugs. Sci Rep. 2019 Nov 28;9(1):17790.

8. Castañeda-Mogollón D, Toppings NB, Kamaliddin C, Lang R, Kuhn S, Pillai DR. Amplicon Deep Sequencing Reveals Multiple Genetic Events Lead to Treatment Failure with Atovaquone-Proguanil in Plasmodium falciparum. Antimicrobial Agents and Chemotherapy. 2023 May 8;67(6):e01709-22.

9. Lerch A, Koepfli C, Hofmann NE, Messerli C, Wilcox S, Kattenberg JH, et al. Development of amplicon deep sequencing markers and data analysis pipeline for genotyping multi-clonal malaria infections. BMC Genomics. 2017 Nov 13;18(1):864.

10. Hathaway NJ, Parobek CM, Juliano JJ, Bailey JA. SeekDeep: single-base resolution de novo clustering for amplicon deep sequencing. Nucleic Acids Research. 2018 Feb 28;46(4):e21.

11. Early AM, Daniels RF, Farrell TM, Grimsby J, Volkman SK, Wirth DF, et al. Detection of low-density Plasmodium falciparum infections using amplicon deep sequencing. Malaria Journal. 2019 Jul 1;18(1):219.

12. LaVerriere E, Schwabl P, Carrasquilla M, Taylor AR, Johnson ZM, Shieh M, et al. Design and implementation of multiplexed amplicon sequencing panels to serve genomic epidemiology of infectious disease: a malaria case study [Internet]. Infectious Diseases (except HIV/AIDS); 2021 Sep [cited 2021 Sep 27]. Available from: http://medrxiv.org/lookup/doi/10.1101/2021.09.15.21263521

13. Okonechnikov K, Golosova O, Fursov M, the UGENE team. Unipro UGENE: a unified bioinformatics toolkit. Bioinformatics. 2012 Apr 15;28(8):1166–7.

14. Taylor SM, Sumner KM, Freedman B, Mangeni JN, Obala AA, Prudhomme O'Meara W. Direct Estimation of Sensitivity of Plasmodium falciparum Rapid Diagnostic Test for Active Case Detection in a High-Transmission Community Setting. Am J Trop Med Hyg. 2019 Dec;101(6):1416–23.

15. Nelson CS, Sumner KM, Freedman E, Saelens JW, Obala AA, Mangeni JN, et al. High-resolution micro-epidemiology of parasite spatial and temporal dynamics in a high malaria transmission setting in Kenya. Nat Commun. 2019 Dec 9;10(1):5615.

16. Köster J, Rahmann S. Snakemake—a scalable bioinformatics workflow engine. Bioinformatics. 2012 Oct 1;28(19):2520–2.

17. Martin M. Cutadapt removes adapter sequences from high-throughput sequencing reads. EMBnet.journal. 2011 May 2;17(1):10–2.

18. Bolger AM, Lohse M, Usadel B. Trimmomatic: a flexible trimmer for Illumina sequence data. Bioinformatics. 2014 Aug 1;30(15):2114–20.

19. Bushnell B. BBMap: A Fast, Accurate, Splice-Aware Aligner [Internet]. Lawrence Berkeley National Lab. (LBNL), Berkeley, CA (United States); 2014 Mar [cited 2023 Jul 14]. Report No.: LBNL-7065E. Available from: https://www.osti.gov/biblio/1241166

20. Callahan BJ, McMurdie PJ, Rosen MJ, Han AW, Johnson AJA, Holmes SP. DADA2: High-resolution sample inference from Illumina amplicon data. Nat Methods. 2016 Jul;13(7):581–3.

21. Robin X, Turck N, Hainard A, Tiberti N, Lisacek F, Sanchez JC, et al. pROC: an open-source package for R and S+ to analyze and compare ROC curves. BMC Bioinformatics. 2011 Mar 17;12(1):77.

22. Bates D, Mächler M, Bolker B, Walker S. Fitting Linear Mixed-Effects Models Using lme4. Journal of Statistical Software. 2015 Oct 7;67:1–48.

23. R Core Team. R: A Language and Environment for Statistical Computing [Internet]. Vienna, Austria: R Foundation for Statistical Computing; 2021. Available from: https://www.R-project.org/

24. RStudio | Open source & professional software for data science teams [Internet]. [cited 2022 Apr 1]. Available from: https://www.rstudio.com/

25. Bodenhofer U, Bonatesta E, Horejš-Kainrath C, Hochreiter S. msa: an R package for multiple sequence alignment. Bioinformatics. 2015 Dec 15;31(24):3997–9.

26. Wickham H, Averick M, Bryan J, Chang W, McGowan L, François R, et al. Welcome to the Tidyverse. Journal of Open Source Software. 2019 Nov 21;4(43):1686.

27. Wickham H, Bryan J, attribution) Rs (Copyright holder of all R code and all C code without explicit copyright, code) MK (Author of included R, code) KV (Author of included libxls, code) CL (Author of included libxls, et al. readxl: Read Excel Files [Internet]. 2019 [cited 2022 Feb 16]. Available from: https://CRAN.R-project.org/package=readxl

28. Paradis E, Schliep K. ape 5.0: an environment for modern phylogenetics and evolutionary analyses in R. Bioinformatics. 2019 Feb 1;35(3):526–8.

29. Hoffman S, Lapp Z, Wang J, Snitkin ESY 2022. regentrans: a framework and R package for using genomics to study regional pathogen transmission. Microbial Genomics. 8(1):000747.

30. Wickham H. Reshaping Data with the reshape Package. Journal of Statistical Software. 2007 Nov 13;21(1):1–20.

570 31. Wickham H, Seidel D, RStudio. scales: Scale Functions for Visualization [Internet]. 2020
571 [cited 2022 Apr 1]. Available from: https://CRAN.R-project.org/package=scales

572 32. Wilke CO. cowplot: Streamlined Plot Theme and Plot Annotations for “ggplot2” [Internet].
573 2019 [cited 2020 Apr 15]. Available from: https://CRAN.R-project.org/package=cowplot

574 33. Ahlmann-Eltze C. ggupset: Combination Matrix Axis for “ggplot2” to Create “UpSet” Plots
575 [Internet]. 2020 [cited 2023 Jul 14]. Available from:
576 https://cran.rstudio.com/web/packages/ggupset/index.html

577 34. Bolker B, Robinson D, Menne D, Gabry J, Buerkner P, Hua C, et al. broom.mixed:
578 Tidying Methods for Mixed Models [Internet]. 2019 [cited 2023 Jul 14]. Available from:
579 https://CRAN.R-project.org/package=broom.mixed

580 35. Aphalo PJ, Slowikowski K. ggpmisc: Miscellaneous Extensions to “ggplot2” [Internet].
581 2018 [cited 2023 Jul 14]. Available from: https://CRAN.R-project.org/package=ggpmisc

582 36. Kassambara A. ggpubr: “ggplot2” Based Publication Ready Plots [Internet]. 2018 [cited
583 2023 Jul 14]. Available from: https://CRAN.R-project.org/package=ggpubr

584 37. Wilke CO. ggtext: Improved Text Rendering Support for “ggplot2” [Internet]. 2020 [cited
585 2022 Apr 1]. Available from: https://CRAN.R-project.org/package=ggtext

586 38. An open dataset of Plasmodium falciparum ... | Wellcome Open Research [Internet].
587 [cited 2023 Jul 14]. Available from: https://wellcomeopenresearch.org/articles/6-42

588 39. Kebschull JM, Zador AM. Sources of PCR-induced distortions in high-throughput
589 sequencing data sets. Nucleic Acids Res. 2015 Dec 2;43(21):e143.

590